

MONITORING IMPERVIOUS SURFACE SPRAWL USING TASSELED CAP TRANSFORMATION OF LANDSAT DATA

Qian Zhang ^{a,*}, Yifang Ban ^a

^a Geoinformatics Division, Dept. of Urban Planning and Environment,
Royal Institute of Technology-KTH, Stockholm, Sweden, 10044 - (qian.zhang, yifang.ban)@abe.kth.se

KEY WORDS: Urban, Monitoring, Change Detection, Transformation, Landsat

ABSTRACT:

Transformation from non-impervious surface to impervious surface changes the landscapes as well as the ecological and environmental conditions. Detecting impervious surface growth is vital to monitoring urban development and supporting sustainable city planning. The objective of this research is to conduct detection of impervious surface sprawl using tasseled cap transformation within the conceptual framework of Vegetation-Impervious surface-Soil (V-I-S) model. Landsat-3 MSS images on August 4, 1979 and Gap-filled Landsat-7 ETM+ images on May 22, 2009, covering the Greater Shanghai Area, were used in the case study. The results demonstrated that direct change detection using variables derived from tasseled cap transformation was effective for monitoring impervious surface sprawl. The variables derived from tasseled cap transformation have the potential to link to the components of the V-I-S model. The Greater Shanghai Area experienced high-speed impervious surface sprawl over the past 30 years at the average speed of 38.84km²/year.

1. INTRODUCTION

The unprecedented combination of economic and population growth has led China into transition from a largely rural society to a predominantly urban one. Monitoring urban dynamic is of critical importance for urban planning and sustainable development in China, especially in the high-speed urbanization regions, such as the Greater Shanghai Area (GSA).

Remote sensing, as a “unique view” of the spatial and temporal dynamics of the processes of urban growth and land use change, has been widely used to monitor land cover changes. Many change detection methods and their improved versions have been investigated widely in the last two decades. Lu et al. (2004) summarized the change detection techniques into seven categories: algebra, transformation, classification, advanced models, GIS-related, visual analysis and other seldom-used techniques. Different approaches have their own advantages and disadvantages. It is impossible to say which approach is absolutely superior to the others, and sometimes different kinds of methods are combined so that the detection result is improved (Jensen, 2005; Seto et al., 2002).

Urban landscapes are a complex mix of buildings, roads, cloverleaf junctions, greenbelts, gardens, exposed soil and water body. In order to understand the heterogeneous landscapes better, the standardized model that describes these component surfaces should be defined. To date, the Vegetation-Impervious surface-Soil (V-I-S) model (Ridd, 1995) is one of the most commonly used conceptual models for remote sensing analysis of urban landscapes. The V-I-S model assumes that land cover in urban areas is a linear combination of three components: vegetation, impervious surface and soil (Figure 1). The diverse nature of these three substances has a significant impact on the dynamics and distribution of energy and moisture flux, the most important drivers in the ecosystem. It is a potentially powerful tool, therefore, for environmental impact analysis of urbanization such as urban heat island analysis (Weng & Lu, 2009). It is also serving as a global standard platform for

spatial-temporal analysis and comparison of urban morphology, biophysical and human systems universally (Ridd, 1995).

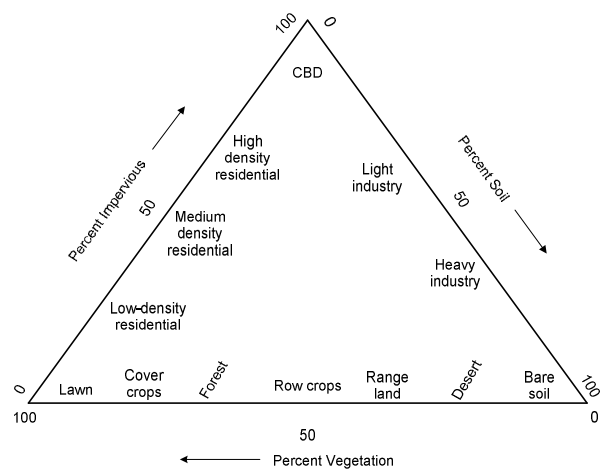


Figure 1. Some urban and near-urban features in the ternary V-I-S model (Ridd, 1995)

Many researchers have experimented with various methods to match the classifications of urban areas with the V-I-S conceptual model. Traditional unsupervised and supervised classification methods, for example, iterative self-organizing data analysis (ISODATA) and maximum likelihood classification (Madhavan et al, 2001); spectral unmixing analysis (Phinn et al., 2002; Weng & Lu, 2009); hierarchy classification (Setiawan et al, 2006; Ward et al., 2000) are the most frequently used methods. The original bands and the bands after principle components analysis (PCA) or minimum noise fraction (MNF) transformation of Landsat TM/ETM+ are the most frequently used data.

Tasseled cap transformation (so called K-T transformation), on other hand, highlights the characteristics of vegetation, and soil,

* Corresponding author

thus may have the potential to be related to the V-I-S components. According to Jensen (2005), urbanized areas are particularly distinct in the brightness component. The greater biomass covering, the brighter the pixel value in the greenness image. The wetness layer provides subtle information about the moisture status of the wetland environment. There has been very little research investigating whether tasseled cap transformation is effective for impervious surface sprawl detection and what is the relationship between variables derived from tasseled cap transformation and the components of the V-I-S model. Thus, there is a need to evaluate whether tasseled cap transformation is an appropriate tool for detecting impervious surface in the conceptual framework of the V-I-S model.

The objective of this research is to conduct detection of impervious surface sprawl in Shanghai using tasseled cap transformation within the conceptual framework of the V-I-S model. The specific aims of this research were: (1) to detect the impervious surface sprawl using tasseled cap transformation; (2) to analyze the spatial-temporal dynamics of impervious surface in GSA over the past 30 years; (3) to determine the relationship between the variables derived from tasseled cap transformation and the components of the V-I-S model.

2. STUDY AREA AND DATA DESCRIPTION

2.1 Study Area

GSA, located in the Yangtze River Delta, Eastern China, was selected as the case study area. It covers approximately 6,430 km² and owns the largest population (18.9 million persons in 2008) among all Chinese cities. Shanghai contributed 4.9% (approximately \$129.5 billion dollars) of national Gross Domestic Product (GDP) in 2006, is one of the most affluent regions in China. During the past 30 years, Shanghai experienced a distinct urban sprawl owing to China's Reform and Open policy, as a result, major land cover transformations took place in Shanghai, where non-impervious surface (for example vegetation, water body, unused land) was replaced by the intensive build-up areas.

2.2 Data Description

To investigate impervious surface sprawl of Shanghai in the past 30 years, Landsat MSS images on August 4, 1979 and ETM+ images on May 22, 2009 were used (Figure 2). Past research has indicated that gap-filled Landsat-7 ETM+ SLC-off data with the USGS EROS released method is an accurate and acceptable data source and likely to produce acceptable classification products and to perform change detection (Bédard, et al., 2008).

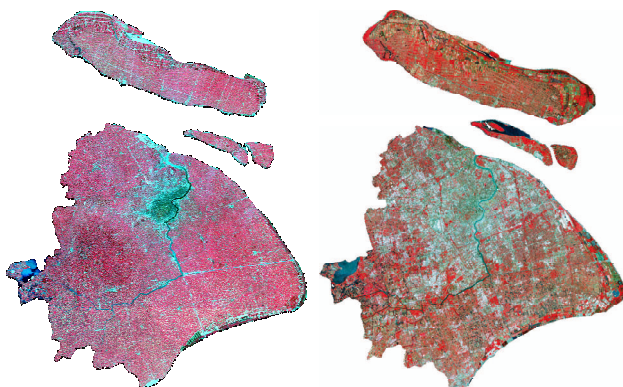


Figure 2. Landsat images of Greater Shanghai Area, China in 1979 (Left, RGB: 321) and 2009 (Right, RGB: 432)

3. METHODOLOGY

3.1 Image Pre-processing

Landsat-7 ETM+ SLC-off data was gap-filled using segment-based method (USGS, 2004). Then the Landsat MSS and ETM+ images were geocoded with a root mean square error (RMSE) approximately 6 m. As a single scene could not cover the whole study area, image mosaicking of two adjacent scenes was carried out and color balance was performed in the overlap region between the two scenes. Then the image was subsetted to the boundary of the GSA.

3.2 Tasseled Cap Transformation (K-T Transformation)

Tasseled cap transformation was developed by Kauth and Thomas in 1976 for Landsat MSS data (Kauth & Thomas, 1976) and was improved and extended to Landsat TM data in the mid-1980s (Crist & Cicone, 1984a; Crist, 1985; Crist & Kauth, 1986). It was widely used in monitoring agriculture, vegetation changes (Collins & Woodcock, 1996; Han et al., 2007; Price et al., 2002; Rogan et al., 2002) as well as urban dynamics detection (Fung, 1990; Seto et al., 2002). Tasseled cap transformation is a kind of orthogonal transformation, it rotates the original data plane so that the vast majority of data variability is concentrated in the features, i.e., the plane is viewed "head-on" and it presents the most basic structures of the data in the most direct way (Crist & Cicone, 1984b). The original Landsat MSS data space was transformed to a new four-dimensional feature space, that is, the soil brightness index (B), greenness vegetation index (G), yellow stuff index (Y), and non-such (N). In this study, we aimed to extract built-up areas information and B, G and Y were derived.

$$\text{Brightness} = 0.332 M_1 + 0.603 M_2 + 0.675 M_3 + 0.262 M_4 \quad (1)$$

$$\text{Greenness} = -0.283 M_1 - 0.660 M_2 + 0.557 M_3 + 0.388 M_4 \quad (2)$$

$$\text{Yellowness} = -0.899 M_1 + 0.428 M_2 + 0.076 M_3 - 0.041 M_4 \quad (3)$$

Where M_{1-4} represent digital numbers (DNs) of band 1 to 4.

For Landsat-7 ETM+ images, Brightness (B), Greenness (G), Wetness (W) and the fourth, fifth, sixth variables were produced and the first three variables were selected. Past research has indicated that at-satellite reflectance-based K-T transformation is needed because changing sun illumination geometry affects DN strongly, and thus affects the derived tasseled cap value. Moreover, at-satellite reflectance-based K-T transformation can differentiate water from land targets better than the DN and reflectance factor based transformation (Huang et al., 2005). DN should, therefore, be converted to at-satellite reflectance firstly according to formulae 3 and 4 (Myeong et al., 2006). After the two steps, the effects owing to different sun angles at different dates were compensated. Correspondingly, the coefficients (Huang et al., 2005) here varied from the DN-based transformation (formulae 5-7).

$$L_\lambda = (DN_\lambda \cdot gain_\lambda) + bias_\lambda \quad (3)$$

Where L is radiance; λ is the spectral band; gain is he spectral band gain; and bias is the spectral band offset.

$$\rho_\lambda = \frac{\pi \cdot L_\lambda \cdot d^2}{E_{sun\lambda} \cdot \cos(\theta)} \quad (4)$$

Where ρ is the unitless in-band planetary reflectance; λ is the spectral band; L is radiance; d is the Earth-Sun distance; E_{sun} is the mean solar atmospheric irradiance; and θ is solar zenith angle in degrees.

$$\begin{aligned} \text{Brightness} = & 0.3561 \rho_1 + 0.3972 \rho_2 + 0.3904 \rho_3 \\ & + 0.6966 \rho_4 + 0.2286 \rho_5 + 0.1596 \rho_7 \end{aligned} \quad (5)$$

$$\begin{aligned} \text{Greenness} = & -0.3344 \rho_1 - 0.3544 \rho_2 - 0.4556 \rho_3 \\ & + 0.6966 \rho_4 - 0.0242 \rho_5 - 0.2630 \rho_7 \end{aligned} \quad (6)$$

$$\begin{aligned} \text{Wetness} = & 0.2626 \rho_1 + 0.2141 \rho_2 + 0.0926 \rho_3 \\ & + 0.0656 \rho_4 - 0.7629 \rho_5 - 0.5388 \rho_7 \end{aligned} \quad (7)$$

3.3 Detection of Impervious Surface Sprawl

3.3.1 Direct Change Detection

Direct change detections were performed using Brightness and Greenness variables from 1979 and 2009. As the transition from non-impervious surface to impervious surface results in big difference in both brightness and greenness, the sprawl area should be concentrated in upper-right part of the 2D scatter plot between Δ Brightness and Δ Greenness (Figure 3a). By adjusting the data range (points in red region of figure 4a) in the plot, the corresponding distribution of points can be highlighted interactively in the image window (Figure 3b). The impervious surface sprawl was then determined with the assistance of field data and the Landsat images.

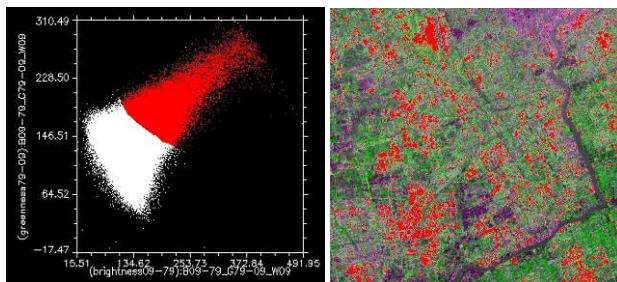


Figure 3(a) 2D scatter plot between Δ Brightness (X-axis) and Δ Greenness (Y-axis) (b) Corresponding regions to red points of 2D scatter plot of Figure 4a

3.3.2 Unsupervised Classification: ISODATA

Unsupervised classification was performed on the changes in Brightness and Greenness using Interactive Self-Organizing Data Analysis (ISODATA). The parameters for ISODATA classification conclude: change threshold is 5%, maximum class stdv is 1.00, minimum class distance is 5.00 and the number of classes is from 5 to 10.

3.4 Accuracy Assessment

For validation of the change detection results, 2000 randomly selected testing points were generated, among which 1000 were for impervious surface sprawl (ISS) and the other 1000 for non-impervious surface (NISS).

4. RESULTS AND DISCUSSION

4.1 Visualization of the Variables from K-T Transform

Figure 4 shows the colour composites of Brightness, Greenness, and Wetness derived from the 2009 ETM+ images. Built-up

areas are highlighted in Red and vegetation is in Green while water is in Blue.

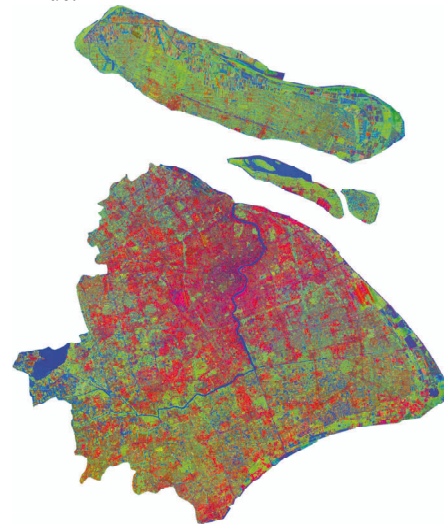


Figure 4. Colour composites map of Brightness, Greenness, and Wetness derived from 2009 ETM+ data

Figure 5 shows the colour composites of Brightness, Greenness, and Yellowness derived from the 1979 MSS images. Built-up areas are shown in blue and orange, vegetation is in Yellow while water is in dark blue, purple and black.

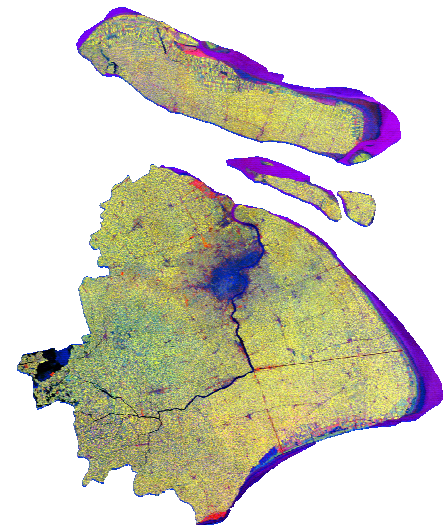


Figure 5. Colour composites map of Brightness, Greenness, and Yellowness derived from 1979 MSS data

Figure 6 is the colour composites of changes in Brightness (in Red and Blue) and Greenness (Green) in 2009. Δ Brightness is derived by brightness 2009 minus brightness 1979 while Δ Greenness is computed by greenness 1979 minus greenness 2009 in order to highlight the impervious surface sprawl. As a result, Δ Brightness above 0 means brightness increases while Δ Greenness above 0 means greenness decreases. Increase in brightness and decrease in greenness is highlighted in white in Figure 6, and the single change in brightness or greenness is highlighted in purple or green correspondingly.

From the observation of Figure 6 with the aid of field investigations, most impervious surface sprawl is related to

white regions except the coastal area. It indicated that, on one side, the impervious surface sprawl can be highlighted well in the color composites of increases in Brightness and decreases in Greenness. Even though the images were acquired in late May and early August respectively, seasonal effects were not significant as both late May and Early August belong to the summer season with the multi-year average temperature in May at 22°C and in August at 28.7°C and vegetation in Shanghai in both months is green. On the other hand, impervious surface sprawl is not characterized in white in shoreline areas. This maybe explained according to Jensen (2005), when conducting change detection in the coastal zone, many influence factors should be considered, such as the different tidal stage.

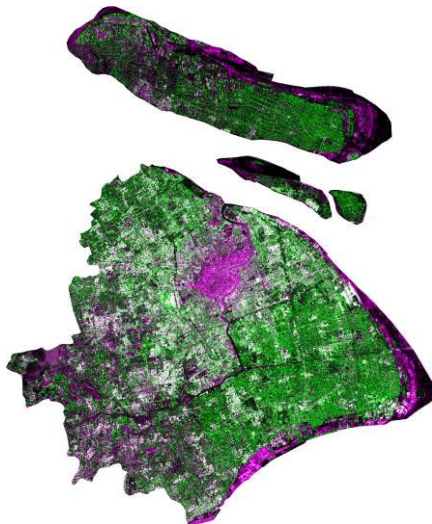
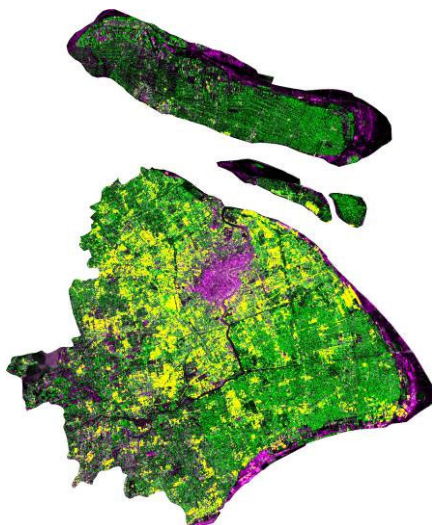


Figure 6. Color composites of Δ Brightness (R), Δ Greenness (G) and Δ Brightness (B)

4.2 Detection of Impervious Surface Sprawl

The direct change detection results using 2-D scatter plot of Brightness and Greenness is shown in Figure 7, with the increase in impervious surface in yellow, and the background map is Figure 6. The accuracy assessment is listed in Table 8. Greater than 90% of the producers' and users' accuracies were achieved and the kappa is 0.84.



Detected sprawl area of impervious surface

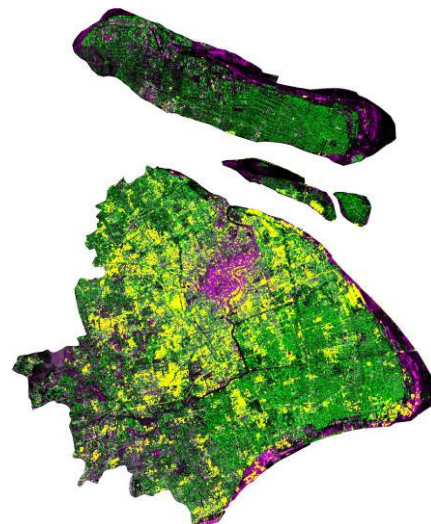
Figure 7. Detected result of impervious surface sprawl using 2D scatter plot

Ref. Res.	ISS	NISS	Total	Producers' Accu.	Users' Accu.
ISS	901	82	983	90.1%	91.7%
NISS	99	918	1017	91.8%	90.3%
Total	1000	1000	2000	91.0%	

Kappa Coefficient= 0.84

Table 8. Accuracy of direct change detection

For the unsupervised classification, seven classes were produced and the 7th class was determined as impervious surface sprawl while the other six classes were recognized as non-impervious surface. The impervious surface sprawl result is presented in yellow in Figure 9. Figure 6 is taken as the background map too. The accuracies were lower than that of the direct change detection (Table 10).



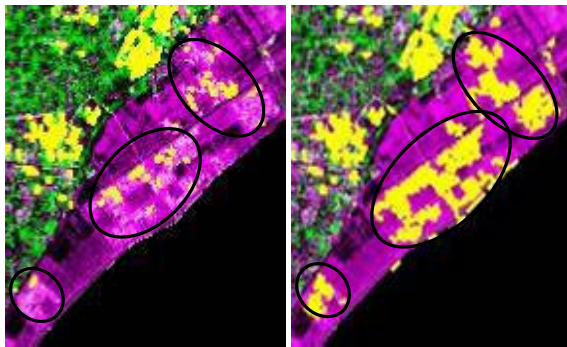
Detected sprawl area of impervious surface

Figure 9. Detected result of impervious surface sprawl using ISODATA unsupervised classification

Ref. Res.	ISS	NISS	Total	Producers' Accu.	Users' Accu.
ISS	851	85	936	85.1%	90.9%
NISS	149	915	1064	91.5%	86.0
Total	1000	1000	2000	88.3%	

Kappa Coefficient= 0.80

Table 10. Accuracy of ISODATA unsupervised classification



Detected sprawl area of impervious surface

Figure 11. Comparison of detection method in shoreline area (a) direct change detection (b) ISODATA classification

Figure 11 shows the comparisons of the two methods in the shoreline regions. Detected impervious surface sprawl was highlighted in yellow. The difference in the ellipse illustrated that ISODATA classification was able to detect nearly all the impervious surface sprawl while the large portion of the impervious surface sprawl was not detected using direct change detection. Visual inspection indicated that in this case ISODATA is superior for detecting impervious surface in the shoreline region even though direct change detection method has the higher overall accuracy than ISODATA. Therefore, the final map of the impervious surface sprawl was a composite of both results with ISODATA result in the shoreline area and direct change detection result in other regions.

The overall accuracy of combined detection method on both ISS and NISS is 92.5%, and the Kappa coefficient is 0.8614. The detected impervious surface sprawl result is shown in Figure 13 and the detailed accuracy is listed in Table 12.

Res. \ Ref.	ISS	NISS	Total	Producers' Accu.	Users' Accu.
ISS	913	63	976	91.3%	93.5%
NISS	87	937	1024	93.7%	91.5%
Total	1000	1000	2000	92.5%	

Kappa Coefficient=0.86

Table 12. Accuracy of hybrid detection method

4.3 The spatial-temporal dynamics of impervious surface in Shanghai

Based on combined result, the temporal-spatial dynamics of impervious surface in GSA over the past 30 years was analyzed. The impervious surface encroached large area of agricultural land and other vegetation (approximate 1165.1km²) over the past 30 years with the extremely high annual expansion speed (38.84 km²/year in average). In addition, Shanghai reclaimed and is reclaiming land from the sea due to many pressures, such as the high land price in the city, and agriculture compensation policy for build-up encroached areas.

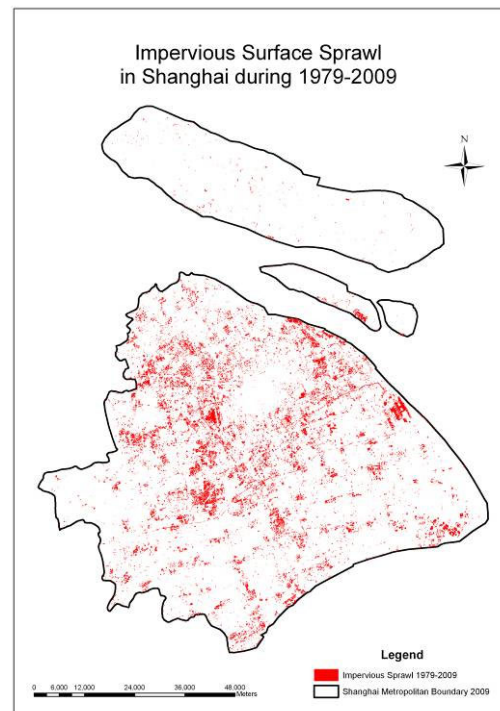


Figure 13. Detection of impervious surface sprawl between 1979 & 2009

4.4 The relationship between Tasseled Cap Variables and the V-I-S Components

In the following 2D scatter plots (Figure 14 a, b), impervious surface, soil and low coverage of vegetation, water body and high coverage of vegetation is expressed in red, yellow, blue and green respectively. The samples are selected using the ground truth points from field work in October, 2009. From the following figures, the different components of the V-I-S model can be illustrated relatively separated in the feature space of tasseled cap variables, for instance Brightness-Greenness space, than the feature space of Landsat ETM+ original bands.

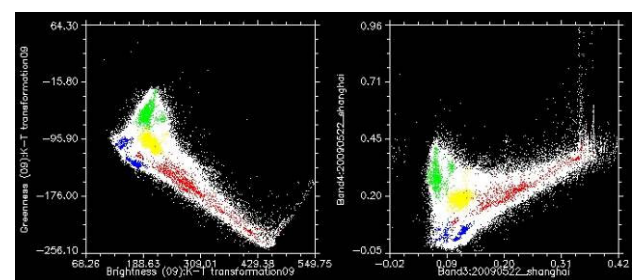


Figure 14 (a). Scatter plot between Brightness (X-axis) and Greenness (Y-axis) in 2009; (b). Scatter plot between Band 3 (X-axis) and Band 4 (Y-axis) of Landsat ETM+, 2009

5. CONCLUSION

This study showed that tasseled cap transformation is an effective method for detecting impervious surface sprawl in GSA and the variables derived from tasseled cap transformation has the potential to link with the components of the V-I-S model. The results also demonstrated that the GSA experienced high-speed impervious surface sprawl over the past 30 years at the average speed of 38.84km²/year.

REFERENCES

- Bédard, F., Reichert, G., Dobbins, R., & Trépanier, I., 2008. Evaluation of segment-based gap-filled Landsat ETM+ SLC-off satellite data for land cover classification in southern Saskatchewan, Canada. *International Journal of Remote Sensing*, 29(7), 2041-2054.
- Collins, J. B., & Woodcock, C. E., 1996. An assessment of several linear change detection techniques for mapping forest mortality using multitemporal landsat TM data. *Remote Sensing of Environment*, 56(1), 66-77.
- Crist, E. P., & Cicone, R., 1984a. Application of the tasseled cap concept to simulated Thematic Mapper data. *Photogrammetric Engineering and Remote Sensing*, 50(3), 343-352.
- Crist, E. P., & Cicone, R. C., 1984b. A physically-based transformation of thematic mapper data---The TM Tasseled Cap. *Geoscience and Remote Sensing, IEEE Transactions on*, GE-22(3), 256-263.
- Crist, E. P., & Kauth, R. J., 1986. The Tasseled Cap De-Mystified. *Photogrammetric Engineering and Remote Sensing*, 52(1), 81-86.
- Crist, E. P., 1985. A TM Tasseled Cap equivalent transformation for reflectance factor data. *Remote Sensing of Environment*, 17(3), 301-306.
- Fung, T., 1990. An assessment of TM imagery for land-cover change detection. *IEEE Transactions on Geoscience and Remote Sensing*, 28(4), 681-684.
- Han, T., Wulder, M., White, J., Coops, N., Alvarez, M., & Butson, C. 2007. An Efficient Protocol to Process Landsat Images for Change Detection With Tasseled Cap Transformation. *Geoscience and Remote Sensing Letters, IEEE*, 4(1), 147-151.
- Huang, C., Wylie, B., Zhang, L., Homer, C., & Zylstra, G., 2005. tasseled.pdf (application/pdf Object). Retrieved September 11, 2009, from <http://landcover.usgs.gov/pdf/tasseled.pdf>
- Jensen, J. R., 2005. *Introductory Digital Image Processing A Remote Sensing Perspective* (3rd ed.). Prentice Hall.
- Kauth, R., & Thomas, G., 1976. The tasseled cap-a graphic description of the spectral-temporal development of agricultural crops as seen by LANDSAT. In *Proceedings of the Symposium on Machine Processing of Remotely Sensed Data* (pp. 4B41-4B51). Presented at the Proceedings of the Symposium on Machine Processing of Remotely Sensed Data, Purdue University, West Lafayette.
- Lu, D., Mausel, P., Brondízio, E., & Moran, E., 2004. Change detection techniques. *International Journal of Remote Sensing*, 25(12), 2365-2401.
- Madhavan, B. B., Kubo, S., Kurisaki, N., & Sivakumar, T. V. L. N., 2001. Appraising the anatomy and spatial growth of the Bangkok Metropolitan area using a vegetation-impervious-soil model through remote sensing. *International Journal of Remote Sensing*, 22(5), 789-806.
- Myeong, S., Nowak, D. J., & Duggin, M. J., 2006. A temporal analysis of urban forest carbon storage using remote sensing. *Remote Sensing of Environment*, 101(2), 277-282.
- Phinn, S., Stanford, M., Scarth, P., Murray, A. T., & Shyy, P. T., 2002. Monitoring the composition of urban environments based on the vegetation-impervious surface-soil (VIS) model by subpixel analysis techniques. *International Journal of Remote Sensing*, 23(20), 4131-4153.
- Price, K. P., Guo, X., & Stiles, J. M., 2002. Optimal Landsat TM - band combinations and vegetation indices for discrimination of six grassland types in eastern Kansas. *International Journal of Remote Sensing*, 23(23), 5031-5042.
- Ridd, M. K., 1995. Exploring a V-I-S (vegetation-impervious surface-soil) model for urban ecosystem analysis through remote sensing: comparative anatomy for cities†. *International Journal of Remote Sensing*, 16(12), 2165-2185.
- Rogan, J., Franklin, J., & Roberts, D. A., 2002. A comparison of methods for monitoring multitemporal vegetation change using Thematic Mapper imagery. *Remote Sensing of Environment*, 80(1), 143-156.
- Setiawan, H., Mathieu, R., & Thompson-Fawcett, M. 2006. Assessing the applicability of the V-I-S model to map urban land use in the developing world: Case study of Yogyakarta, Indonesia. *Computers, Environment and Urban Systems*, 30(4), 503-522. doi:10.1016/j.compenvurbsys.2005.04.003
- Seto, K. C., Woodcock, C. E., Song, C., Huang, X., Lu, J., & Kaufmann, R. K. 2002. Monitoring land-use change in the Pearl River Delta using Landsat TM. *International Journal of Remote Sensing*, 23(10), 1985-2004.
- USGS. 2004. SLC-off Gap-Filled Products Gap-Fill Algorithm Methodology. Retrieved September 11, 2009, from <http://landsat.usgs.gov/documents/L7SLCGapFilledMethod.pdf>
- Ward, D., Phinn, S. R., & Murray, A. T. 2000. Monitoring growth in rapidly urbanizing areas using remotely sensed data. *Professional Geographer*, 52(3), 371-386.
- Weng, Q., & Lu, D. 2009. Landscape as a continuum: an examination of the urban landscape structures and dynamics of Indianapolis City, 1991–2000, by using satellite images. *International Journal of Remote Sensing*, 30(10), 2547-2577.

ACKNOWLEDGEMENT

This research was also supported by grants from the Swedish Science Foundation (VR), the Swedish Science Foundation and the Swedish Research Council for Environment, Agricultural Sciences and Spatial Planning (FORMAS) awarded to Professor Ban.